Colloids and Surfaces A 598 (2020) 124815

Contents lists available at ScienceDirect

Colloids and Surfaces A

journal homepage: www.elsevier.com/locate/colsurfa

Formation and stabilization of CO_2 bubbles with different sizes and the interaction with solid particles

Xiaohan Zhang, Haoyang Sun, Hui Zhao, Yan Qin, Qiaozhi Wang, Ying Li*

Key Laboratory of Colloid and Interface Chemistry of State Education Ministry, Shandong University, 27 South Road of ShanDa, Jinan, Shandong, 250100, PR China

GRAPHICAL ABSTRACT

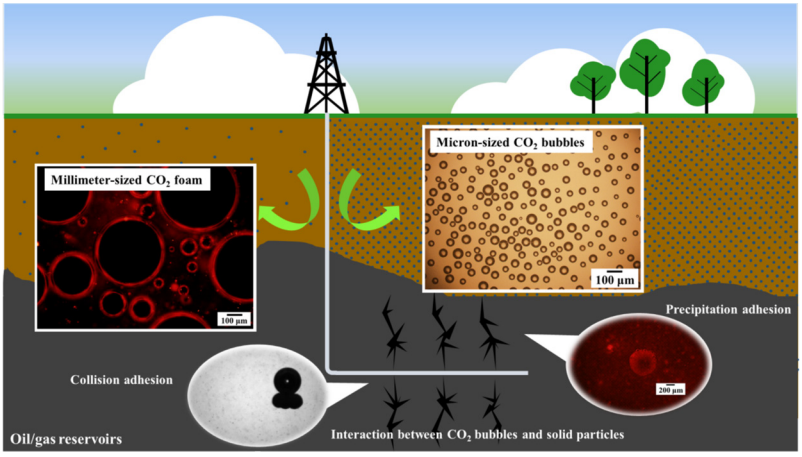

ARTICLE INFO

Keywords:
CO_2 bubbles
HMPE
Foam fracturing fluids
EOR/EGR
Solid particles
Settling velocity

ABSTRACT

Various applications of CO_2 have received extensive attention, especially those realizing the reuse of the greenhouse gas and meeting the application requirements simultaneously, of which the CO_2 enhanced oil recovery (EOR) and enhanced gas recovery (EGR) approaches is a paradigm. In recent years, the applications of CO_2 foam as flooding or fracturing system are both of the research hotspots. Since conventional surfactants are generally poor in stabilizing CO_2 foam, the exploration of CO_2 foam stabilizer is of great significance, while it is also a difficult problem. In this work, a kind of hydrophobically modified water-soluble polyelectrolyte (HMPE) was used in the stabilization of CO_2 foam containing millimeter-sized and micron-sized bubbles, which both exhibit high stability and perfect foam viscoelasticity, due to the enhancement of the mechanical strength of the foam films through HMPE absorbed at the gas/liquid interfaces. The interaction between the CO_2 bubbles and ceramiste particles was investigated, the mechanism of the excellent sand-carrying performance of the CO_2 foam system was discussed. Based on the comprehensive understanding of all aspects of the properties, the HMPE-CO_2 foam system has bright potential being used in the CO_2-foam fracturing.

* Corresponding author.
E-mail address: yingli@sdu.edu.cn (Y. Li).

https://doi.org/10.1016/j.colsurfa.2020.124815
Received 23 January 2020; Received in revised form 31 March 2020; Accepted 2 April 2020
Available online 12 April 2020

1. Introduction

Currently, due to the continuous depletion of conventional oil and gas reservoirs, the intensive development of unconventional reservoirs, for instance, the ultra-low permeability oil/gas reservoirs, have important significance to meet the expanding demand for petroleum and natural gas [1–5]. CO_2 enhanced EOR and EGR has been recognized as an alternative and highly beneficial method, and economic utilization of greenhouse gases contributes to the carbon sequestration, which has aroused much more attention [6–9]. On the one hand, CO_2 can dissolve into oil, significantly reduce the interfacial tension and oil viscosity, and improve the mobility ratio during CO_2 flooding. On the other hand, CO_2 has relatively high adsorption capacity on surface of diverse reservoir minerals, which can effectively release the adsorbed shale oil or gas, enhancing the oil/gas recovery [10,11].

However, due to the low density and low viscosity of CO_2, gas channeling and gravity segregation usually occur under reservoir conditions during CO_2 flooding, which result in the low sweep efficiency [12–14]. CO_2 foam flooding could improve the mobility ratio and diverts CO_2 to the relatively low-permeability zones or fractures, enhancing the sweep efficiency adequately as a result of the higher apparent viscosity of CO_2 foam [15]. Similarly, CO_2 foam fracturing technology could conquer the limitation in practical applications caused by the low viscosity and density of CO_2 [16,17], and exhibit excellent proppant transport ability and quick flowing back [18], which is suitable for exploiting both oil and gas reservoirs. Besides, due to the small liquid content, CO_2 foam fracturing fluids could reduce the potential damage to sensitive reservoir and has less fluid loss than that of conventional fracturing fluid [19,20]. Thereby CO_2 foam flooding and foam fracturing are both technically feasible ways to overcome the shortcoming of CO_2 injection.

The generation of stable CO_2 foam is the key problem for the application, while is still a big challenge [19,21]. Because CO_2 molecules can easily pass through the barrier layer of surfactants in the foam films, leading to the easy coalescence and rupture of bubbles [22], the stability of CO_2 foam stabilized only by conventional surfactants is not always satisfactory, especially under the harsh reservoir conditions with high temperature or high salt concentration [23]. In order to improve the CO_2 foam stability, different composite systems have been explored in the current researches [24–27]. Diverse nanoparticles such as SiO_2, $CaCO_3$, Fe_2O_3, fly ash, and biological origin micro particles [28–35], and water-soluble polymers such as hydrolyzed polyacrylamide, xanthan gum [36,37], have been explored to enhance the foam stability of surfactant. It was found that the nanoparticles-surfactant composite can stabilize CO_2 foam due to the adsorption of nanoparticles on the bubble surface [38], preventing the coalescence, disproportionation of the bubbles, and the liquid drainage of the foam membrane [13,39]. The polymers could increase the apparent viscosity of the solution, which slows down liquid drainage of the CO_2 foam [36] and the polymer/surfactant network formed in the foam liquid film is beneficial for improving the surface strength of the lamella, and reducing the film permeability [40]. However, because of the high price, complexity of the technology, as well as the lack of understanding on the mechanisms, foams stabilized by the composite of surfactants and particles or polymers are not yet feasible to be widely implemented in the field of EOR and EGR [41]. The exploration of CO_2 foam stabilizer is still a challenge.

Besides, as for the recovery of the unconventional reservoirs, such as shale oil and gas, the preparation of high-performance CO_2 foam systems remains more tough challenges, one of which is how to generate small-sized CO_2 bubbles with ideal stability. The current studies are all about apparent foams, in which the bubble size is in mm scale, but few studies have been done on the generation of small-sized CO_2 foam, good performance system and the theoretical understanding are both lacking.

In this paper, hydrophobically modified water-soluble polyelectrolyte (HMPE) was selected as the foam stabilizer, gas flow method and pressurization-decompression method were used to produce millimeter-sized and micron-sized CO_2 bubbles respectively. The static stability, dynamic stability and rheological properties of the formed CO_2 foam system were investigated. The affecting factors and the mechanism of bubble generation and stabilization were analyzed. The load capacity of the produced CO_2 foam to ceramsite and the settling velocity of ceramsite particles in CO_2 foam system were determined, the mechanism of CO_2 bubbles carrying the solid particles was discussed, which showed a good application prospect of HMPE stabilized CO_2 foam system being used in the foam fracturing.

2. Materials and methods

2.1. Materials

Hydrophobically modified water-soluble polyelectrolyte (HMPE) with the average molecular weight of 100,000 was formed by grafting a hydrophobic carbon chain on the hydrophilic segment of polyacrylic acid, of which the ingredient ratio of hydrophobic modified segments is 10%. The detailed preparation method of HMPE were specified in the previous work of our lab [42]. The fluorescent indicator Rhodamine B (purity > 99%) was purchased from Aladdin. Ultra-pure water with a resistivity of 18.2 MΩ cm was used in the solution preparation.

2.2. Preparation of HMPE solution

Stock solution of 1.0 wt% HMPE was prepared by dissolving 1.0 g of solid powder in 100 g H_2O. HMPE solution at low concentrations were obtained via dilution of the stock solution. During the preparation of the solution, each concentration of HMPE solution must be stirred for 24 h to ensure that the polymer molecules are completely dissolved in the solution. The pH of the HMPE solution was 4.0 ± 0.1, which had not been adjusted.

2.3. Bulk phase viscosity

The bulk phase viscosity of HMPE solution was measured by a Brookfield R/S plus rheometer at a fixed shear rate, using a CC3-40 cylinder measuring system. The rotor type was MB3-40F drum, and the shear rate was 200 s^{-1}. The temperature was controlled at 50°C.

2.4. Equilibrium surface tension

The equilibrium surface tension of surfactant systems was measured on a K100 apparatus (KRÜSS GmbH, Hamburg) using the Wilhelmy plate method. The surface tension of Milli-Q water (72.8 mN/m) was measured in order to ensure the accuracy of the instrument. The metal plate need to be burned using alcohol to remove the impurities of the surface. The HMPE solution needed to stand for at least 10 min after being placed in the measuring tank to ensure that the HMPE macromolecules can be completely adsorbed on the gas/liquid interface, so as to obtain the accurate surface tension values. The device was calibrated and cleaned using Milli-Q water.

2.5. Formation of CO_2 foam

The gas flow method. The 50 mL HMPE solution was poured into the sand core glass tube with interlayer, which is connected with water bath, the temperature was kept at 50°C. CO_2 was bubbled into the solution with a constant gas flow rate of 100 mL/min under ambient pressure. When the foam rose to the scale value of 200 mL, the foaming was stopped, then the change process of the foam volume with time was recorded. The corresponding time was the half-life of the foam when the foam volume decayed to half of the initial volume. The half-life time represented the better the static stability of CO_2 foam.

The pressurization-decompression method. Firstly, 50 mL HMPE

solution was poured into the high-pressure resistant reactor, and the pressurization device was connected with the reactor by pressing down the handle to inject CO_2 gas into the reactor. HMPE solution was saturated with CO_2 gas under a certain pressure and time. Then, the reactor was slowly released pressure causing a massive bubble nucleation in the solution. Finally, the foam was collected into a graduated container, and the volume expansion ratio and half-life were measured by monitoring with time. The schematic diagram of the device for generating CO_2 bubbles by the pressurization-decompression method as shown in Fig. 6a.

2.6. Observation of foam drainage and coalescence

The FoamScan (Foamscan IT Concept, Teclis Co., France) apparatus was used to observe the process of foam drainage and coalescence. The 60 mL sample was introduced into a reservoir at the bottom of a glass column, CO_2 was bubbled into the solution through a porous disk (pore sizes: $40-100\,\mu m$) with a constant flow rate of 100 mL/min. The temperature was controlled at 50℃. The changing of the liquid fraction in the foam column over time was measured by the first pair of electrodes (located at the bottom of the glass column). The cell size analysis (CSA) camera was utilized to recorded pictures of the CO_2 foam.

2.7. Dynamic stability of CO_2foam

The dynamic foam stability in response to a disturbance was measured by combining a bubble-generating device with a viscometer or a rheometer. The viscosity of CO_2 foam at shear rate of 10 s^{-1} was determined using a Brookfield R/S plus rheometer with a paddle rotor (V40-20 3tol type) at 50℃. The 30 mL HMPE solution was poured into a transparent glass column with a porous filter. The foams were generated by flowing CO_2 into the solution with a constant gas flow rate of 100 mL/min under ambient pressure. When the foam rose to the scale value of 180 mL, the foaming was stopped.

2.8. Rheological properties of CO_2foam

The dynamic viscoelastic measurements of CO_2 foam were performed on a MCR 302 rheometer (Anton Paar, Austria) with a paddle-shaped rotor (ST22-4V-40) at 50℃. The CO_2 foam was obtained by mechanically stirring 200 mL HMPE solutions using Waring blender (1500 mL) at 1000 rpm for 1 min, and saturating in a CO_2 atmosphere for 30 min in advance. The linear viscoelastic regions of CO_2 foam were determined via oscillating stress sweep (0.01–10 Pa) at a frequency of 1 Hz. The variation of moduli with time was obtained at a fixed frequency (1 Hz) and stress (0.02 Pa) until the rotor was exposed.

2.9. Texture analysis

The microhardness and the viscoelastic feature of CO_2 foam were measured using a TMS-Pilot texture analyzer (TL-Pro testing system, FTC, USA). The CO_2 foam was obtained by mechanically stirring 200 mL HMPE solutions using Waring blender (1500 mL) at 1000 rpm for 1 min, and saturating in a CO_2 atmosphere for 30 min in advance. Then, the foam was immediately poured into a cylindrical cell (150 mm inner diameter), and the cell was placed on the sample platform. Subsequently, the extrusion disk with a diameter of 100 mm was controlled by the computer workstation to depress the foam at a constant speed of 20 mm/min. When the extrusion disk reached the preset position, it returned to its departure place. Over the whole process, the pressure variation of the disk was sensed and recorded. The maximum compressing force and viscoelastic force represent the compressing and dragging peak pressures in the falling and pulling procedures which qualitatively correspond to the stiffness and the viscoelasticity of the foam, respectively.

2.10. Microscopicimages of CO_2foam

To observe microstructural changes of CO_2 foam prepared by HMPE solution and the interaction of CO_2 bubbles and ceramsite particles, images were obtained using Olympus BX53 Microscope (Olympus, Japan). For fluorescence observation, Rhodamine B (0.0002 wt%) was used as the fluorescence label of the polymer chain. Green filter was utilized for imaging. The software Image J was used to analyze the images.

2.11. Ceramsite suspension ability test

The static sedimentation velocity of ceramsite was determined. Mixed 20/40 mesh ceramsite (particle size: 425–850 μm) was used to determine the loading value with freshly prepared foam. The total setting distance was 31 cm, and the total foam volume was 55 mL. The ceramsite was evenly added into the top 5 mL foam layer to ensure that the ceramsite reached a constant velocity when it reached the measurement area. The ceramicite level was monitored. The diameter of the measuring cylinder was at least 30 times larger diameter than the diameter of ceramicite so that the particles settling velocity had no effect with confining walls of the cylinder. The ceramsite sedimentation speed was determined visually by measuring the percentage (height) of ceramsite sedimentation with time. A 100% suspension was defined when no ceramsite was found to settle down with time, while 0% ceramsite suspension is applicable for complete sedimentation of ceramsite. The sedimentation time of ceramsite from 50 mL scale line to 0 mL scale line was recorded to calculate the ceramsite settling velocity.

3. Results and discussion

3.1. Formation and stabilization of CO_2foam generated by the gas flow

Fig. 1a shows the bulk phase viscosity of HMPE solution as a function of concentration, the critical association concentration (CAC) is about 0.14 wt%. The increase of the bulk phase viscosity is helpful to enhance the liquid carrying capacity of the CO_2 foam generated from HMPE solution and slow down the liquid drainage. The surface tension with different concentrations of HMPE solution is investigated, as shown in Fig. 1b. It is found that the surface tension of HMPE solution declined with increasing concentration, and could reach as low as 45 mN/m when the concentration is 0.10 wt%. Rhodamine B is used as a fluorescent probe to label HMPE molecules, from the fluorescence microscope image as shown in Fig. 1c, it can be observed that HMPE molecules adsorb at the CO_2/liquid interface to form a thick “armor” surrounding the bubbles, which hinted the potential capability in improving the stability of the CO_2 foam by effectively slowing the diffusion of CO_2 between the bubbles.

The half-life time of the CO_2 foams formed from HMPE solutions with different concentrations is shown in Fig. 1d. It could be found that the static stability of the HMPE-CO_2 foam is excellent. The half-life time of the CO_2 foams increase gradually with HMPE concentration increasing, reaches 350 min for CO_2 foam generated from 0.10 wt% HMPE solution, which is several or even dozens of times longer than that reported by other references [17,22,43,44].

Fig. 2 shows the micrographs of the CO_2 foam in the evolution process. In 120 min, there is only a little change in the bubbles size and number, showed that the coalescence caused caused by Oswald Ripening and rupture of the thin foam film was restrained by the HMPE molecules adsorbed at the surface. It could be also observed that, the average thickness of the bubble shell changed from about 94 μm to less than 58 μm during 120 min, while the shape of bubbles keep being spherical. According to the fluorescence microscope image in Fig. 3(a), when the concentration of HMPE is 0.10 wt%, the bubble shell boundary is very clear. Combining with Fig. 1(b), it could be concluded that in this case almost all of the HMPE molecules adsorb at the bubble

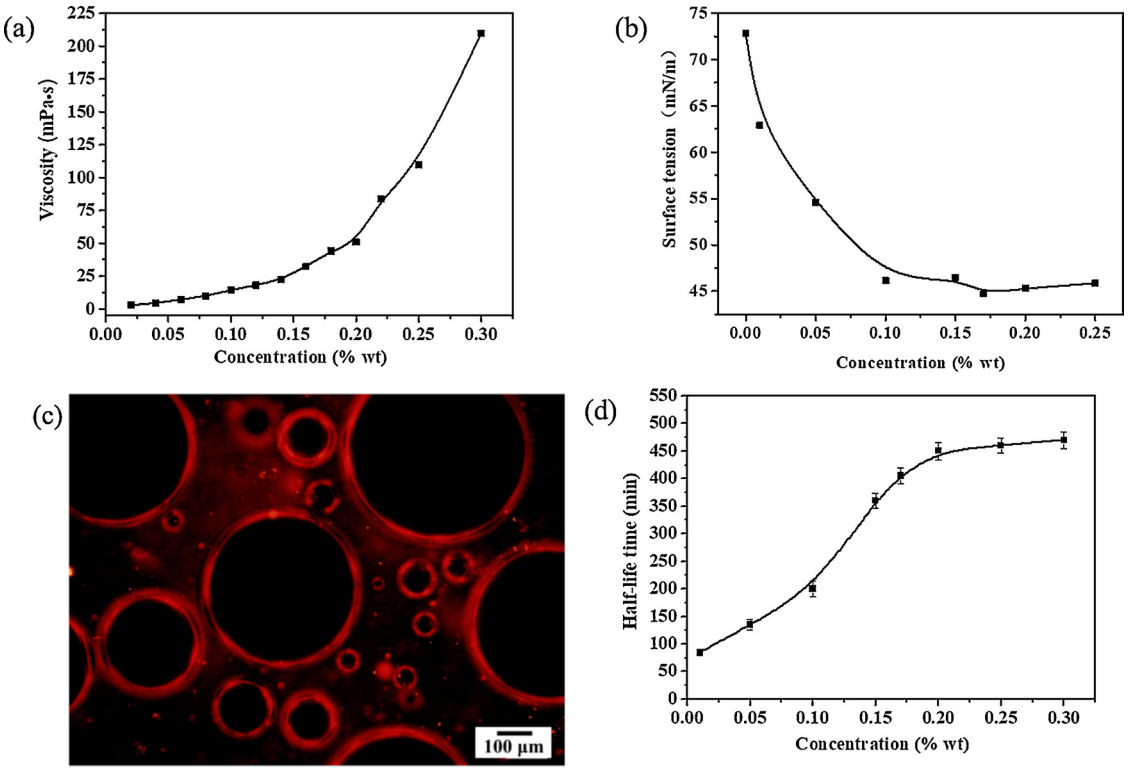

Fig. 1. (a) The viscosity of HMPE solution as a function of the HMPE concentration; (b) the surface tension of HMPE solution as a function of the HMPE concentration; (c) the fluorescence microscope image of CO_2 foam generated from 0.10 wt% HMPE solution; (d) half-life time of the CO_2 foam generated from HMPE solution as a function of concentration at 50℃.

surface, the intermolecular crosslinking did not occur, and the HMPE molecules adsorbed on the bubble surface could gradually array more orderly. When the concentration of HMPE was 0.15 wt%, which exceeds the CAC value, as it was shown from the fluorescence microscope image in Fig. 3(b), the boundary of the bubble shell got unclear, the overlapping of the HMPE molecules both in bulk phase and on interfaces of different bubbles lead to the cross-linking between adjacent CO_2 bubbles, which corresponding to the abrupt increasement of the overall viscosity and liquid carry capacity.

Fig. 3c shows the variation of the liquid fractions of the CO_2 foam generated from 0.10 % wt and 0.15 wt% HMPE solution with time, the results agrees very well with the above discussion. It can be seen that the liquid fraction in the CO_2 foam liquid film produced by 0.10 wt% HMPE remain above 10% after 2000s of liquid drainage, indicating that the strong liquid holding capacity of HMPE. While the duration of the drainage process of CO_2 foam produced by 0.15 wt% HMPE solution is longer, and the liquid fraction after complete drainage could be as high as more than 30%.

The dynamic apparent viscosity of CO_2 foam as function of time under shearing was determined at 50℃, the result is shown in Fig. 4a. The high retention value of dynamic apparent viscosity is maintained in a long period, e.g., the apparent viscosity of CO_2 foam stabilized by 0.10 wt% HMPE solution is 1.6 Pa·s at 1600 s, which is valuable to meet the demand in practical applications. The CO_2 foam formed by 0.15 wt % HMPE solution maintain higher dynamic apparent viscosity, while the higher frictional resistance might be not advantage. Fig. 4b shows the dynamic moduli of CO_2 foam as function of time. Obviously, G' is larger than G'' for the CO_2 foam stabilized by HMPE, indicating a remarkable elastic character.

The compression force and viscoelastic force of CO_2 foam film is measured, as shown in Fig. 5. It can be seen that the CO_2 foam prepared by HMPE solution is much larger than the conventional surfactant-based foam in terms of compressive force and viscoelastic strength [45]. These results demonstrate that a viscoelastic shell was formed by the HMPE molecules adsorbed at the bubbles surface, which enhanced the mechanical strength of the foam films, not only play important role in enhancing the foam stability, but also would be conductive to strengthen the capability of the foam film in loading and transport of proppant, so the HMPE-CO_2 foam has bright potential being used as fracturing fluid.

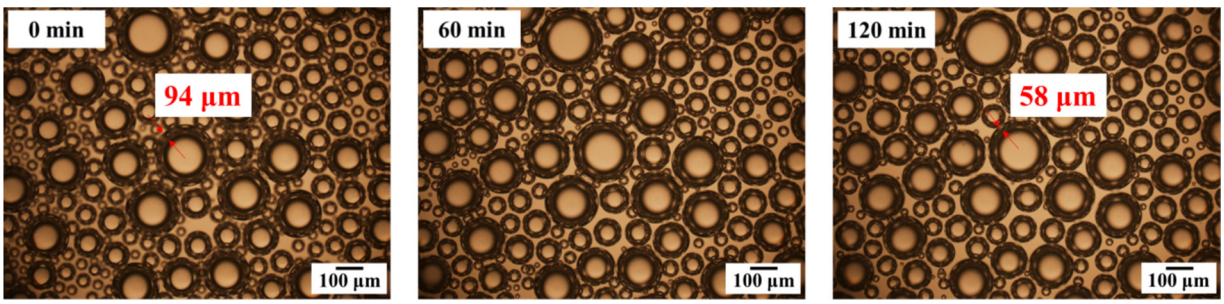

Fig. 2. Microscopic images of the CO_2 foam generated from 0.10 wt% HMPE solution after drainage.

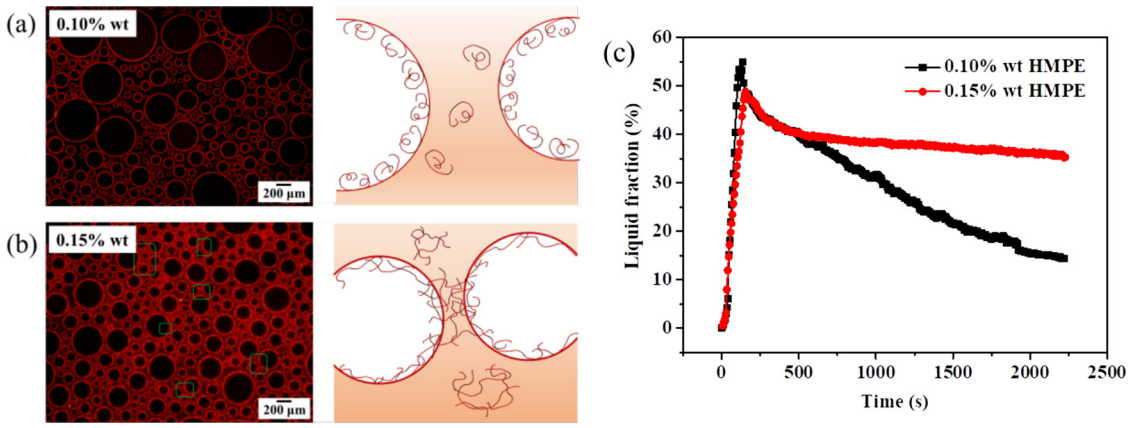

Fig. 3. (a) The fluorescence microscope images and schematic diagram of CO_2 foam generated from 0.10 wt% HMPE solution; (b) the fluorescence microscope images and schematic diagram of CO_2 foam generated from 0.15 wt% HMPE solution; (c) change in the liquid fractions of CO_2 foam as function of time at 50°C. The concentrations of HMPE solution are % wt and 0.15 0.10 wt% and 0.15 wt%, respectively.

Combined with the above results, it could be draw a conclusion that, though the increasement of the overall viscosity and liquid carry capacity is beneficial for the increasement of the foam stability, as shown in Fig. 1(d), the bigger concentration of HMPE is not the better for the practical application for EGR and EOR. Close to but not bigger than CAC would be the suitable concentration for HMPE stabilizing foam, mean while avoiding the performance reduction might be caused by the friction increase of the foam fluid.

3.2. Formation of CO_2bubbles generated by the pressurization-decompression

Considering that the pore size of unconventional reservoirs such as shale is relatively small, small-sized bubbles should be generated to form foam flow to reduce friction, when being used as fracturing fluid for EGR. The pressurization-decompression method is used to form CO_2 microbubbles.

Fig. 6a shows the microscopic images of CO_2 bubbles formed in 0.10 wt% HMPE solution by the pressurization-decompression method. HMPE solution is saturated with CO_2 gas by keeping for 1 h at different equilibrium pressures. When the pressure is reduced to atmospheric pressure, massive CO_2 microbubbles would be formed in the solution. The diameter of the bubbles is observed under microscope, which is found to be about 30–50 μm. With the increase of the equilibrium pressure, the amount of CO_2 bubbles increases significantly, while there is almost no difference in size as shown in Fig. 6b.

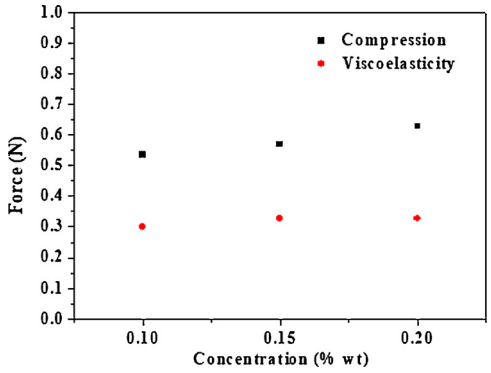

Fig. 5. TA results of CO_2 foam film as function of HMPE concentration.

3.3. Discussion about the formation mechanism of CO_2bubbles generated by the pressurization-decompression

The generation process of the CO_2 bubbles by pressurization-decompression method can be divided into three stages: gas supersaturation, bubble nucleation, bubble growth.

CO_2 can be dissolved in HMPE solution by pressurizing to equilibrium pressure according to Henry's law. Under the supersaturation situation, the amount of the actual dissolved gas in the solution is higher than the dissolved gas amount in the thermodynamic equilibrium state, so the dissolved CO_2 cannot be precipitated immediately

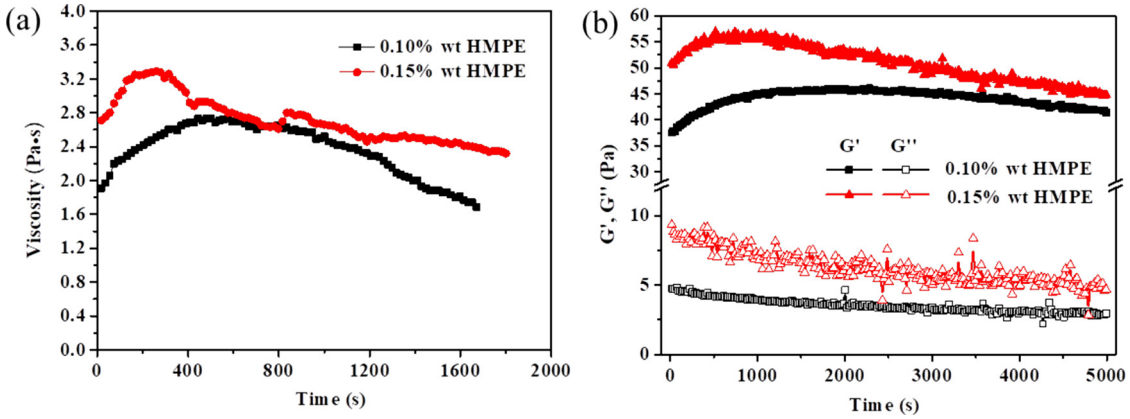

Fig. 4. (a) Apparent viscosity (10 s^{-1}) of CO_2 foam as function of time at 50°C. The concentrations of HMPE solution are % wt and 0.15 0.10 wt% and 0.15 wt%, respectively; (b) Elastic (G') and viscous (G") modulis of CO_2 foam as function of time at 50°C. The concentrations of HMPE solution are % wt and 0.15 0.10 wt% and 0.15 wt%, respectively.

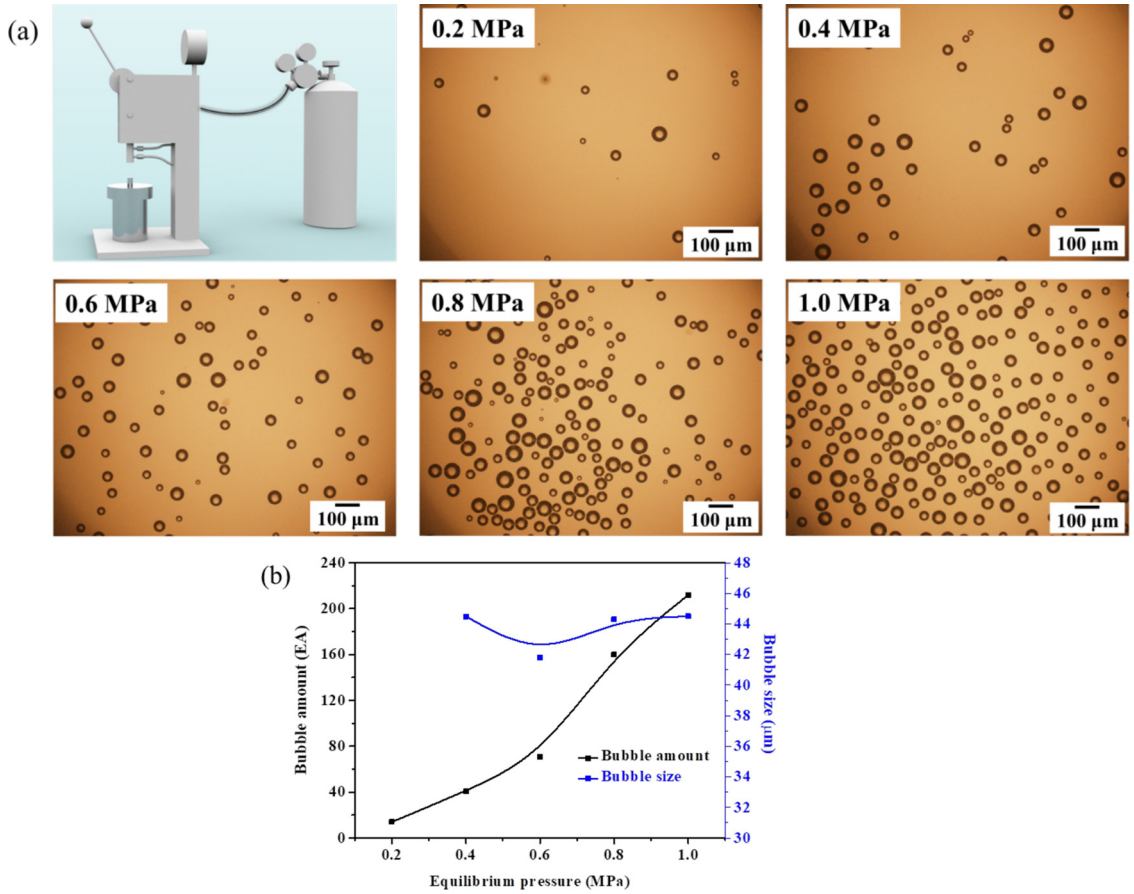

Fig. 6. (a) The schematic diagram of the device for generating CO_2 bubbles by the pressurization-decompression method and the microscopic images of CO_2 bubbles stabilized by 0.10 wt% HMPE solution at different equilibrium pressure; (b) bubble amount and bubble size as a function of equilibrium pressure, when equilibrium pressure was 0.2 MPa, 0.4 MPa, 0.6 MPa, 0.8 MPa and 1.0 MPa respectively.

when the pressure is released. Supersaturation is the driving force of bubble nucleation and growth, and is a necessary condition for bubble formation.

Bubble nucleation includes homogeneous nucleation and heterogeneous nucleation. The premise of homogeneous nucleation is to ignore the influence of impurities and porous impurities as shown in Fig. 7a. According to the classical nucleation theory, the free energy change of bubble nucleation is calculated as follows in Eq. (1):

$$\Delta G = -V_g \Delta p + A_{gl}\gamma_{gl} \quad (1)$$

Where ΔG is the free energy change of bubble nucleation, J; V_g is the volume of bubble nucleus, m^3; Δp is the internal-external pressure difference of bubble nucleus, MPa; A_{gl} is the bubble surface area, m^2; γ_{gl} is the surface tension of the bubble, N/m. For spherical bubble nucleus, further conversion to get the formula as follows in Eq. (2):

$$\Delta G = -\frac{4}{3}\pi r^3 \Delta p + 4\pi r^2 \gamma_{gl} \quad (2)$$

Where: r is the radius of bubble nucleus, m.

ΔG increases during the initial stages of bubble nucleation and decreases when ΔG reaches the critical free energy change ΔG^*. The bubble radius at the critical free energy change ΔG^* is the critical bubble radius r^*. Only when the bubble radius exceeds r^*, the CO_2 bubble is stimulated at a specific pressure drop, and then continues to grow into microbubble by diffusion; otherwise, CO_2 bubbles formed will collapse rapidly and redissolve into the solution.

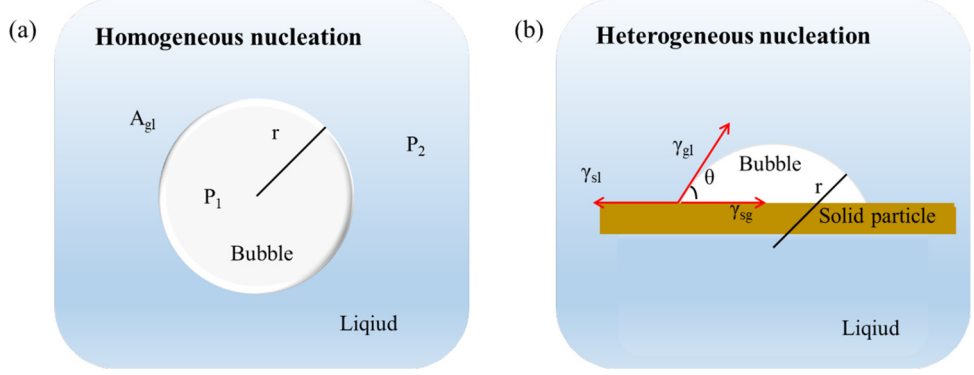

Fig. 7. The schematic diagram of bubble nucleation: (a) homogeneous nucleation; (b) heterogeneous nucleation.

When r = r*, $\frac{dG}{dr} = 0$, take derivation of this expression, as follows in Eqs. (3) and (4):

$$r^* = 2\frac{\gamma_{gl}}{\Delta p} \tag{3}$$

$$\Delta G^* = \frac{16\pi\gamma_{gl}^3}{3\Delta p^2} \tag{4}$$

From the above equation, it can be seen that the critical free energy change and critical bubble radius required for the formation of stable bubbles can be reduced by reducing the surface tension or increasing the internal-external pressure difference of bubble (i.e., saturation). In practice application, higher supersaturation affected by the pressure decay rate can be used to form stable foam.

As shown in Fig. 7b, the nucleation of CO_2 bubbles on the surface of smooth solid particles is heterogeneous nucleation. The free energy change of heterogeneous nucleation is calculated as follows in Eq. (5):

$$\Delta G_{het} = -\frac{4}{3}\pi r^3 \Delta p + 4\pi r^2 \gamma_{gl} \cdot F(\theta) \tag{5}$$

Where, ΔG_{het} is the free energy change of heterogeneous nucleation, J; $F(\theta) = \frac{1}{4}(2 + \cos\theta)(1 - \cos\theta)^2$, θ is the interface wetting angle, rad.

Substitute the critical bubble radius $r^* = 2\frac{\gamma_{gl}}{\Delta p}$ into Eq. (5) to obtain the critical free energy change $\Delta G_{het}{}^*$ of heterogeneous nucleation, as shown in Eq. (6):

$$\Delta G_{het}{}^* = \frac{16\pi\gamma_{gl}^3}{3\Delta p^2} \cdot F(\theta) \tag{6}$$

Comparing Eqs. (4) and (6), $\Delta G_{het}{}^* = \Delta G^* \cdot F(\theta)$ is obtained. Heterogeneous nucleation needs less free energy than homogeneous nucleation because of $F(\theta) \leq 1$. Heterogeneous nucleation will take place preferentially at the same conditions, which is consistent with the experimental results.

Bubble growth includes the mass transfer from dissolved CO_2 gas to microbubble nucleus and the expansion of gas with reduced pressure. The driving force for growth comes from the internal pressure of bubbles, and the resistance comes from the viscosity of solution and the external pressure.

3.4. Stabilization of CO_2bubbles by the pressurization-decompression method

Fig. 8a shows the statistical results of CO_2 bubble amount and bubble size as a function of time. It can be seen that the size of the CO_2 bubbles gradually decreases with time. Therefore, the decay of CO_2 bubbles is caused by the diffusion of CO_2 gas to the liquid phase. In addition, the thickness of bubble liquid film basically remains unchanged, at 17 μm. CO_2 bubbles exist stably in solution without forming foam layer, and the liquid carrying capacity of bubble liquid film is weak, which leads to a thin thickness of liquid film.

The test is based on the generation of foam layer by nucleation of CO_2 bubbles after depressurization of a saturated liquid phase. The volume expansion ratio and half-life time of CO_2 foam layer is shown in Fig. 8b. At first, HMPE molecules are arranged more and more tightly at the gas/liquid interface with the increase of HMPE solution concentration, which makes the volume expansion ratio and half-life time increases gradually. As the HMPE concentration further increased, the viscosity of HMPE solution increases, resulting in an increase the resistance of bubble growth, thereby the volume expansion ratio and half-life time of CO_2 foam layer decreases. The variation trend of volume expansion ratio and half-life time with equilibrium pressure is shown in Fig. 8c. When equilibrium pressure is less than 0.6 MPa, only a small amount of CO_2 foam layer is produced, which is not enough to record. When equilibrium pressure exceeds 0.6 MPa, the volume expansion ratio and half-life time of CO_2 foam layer gradually increase as the pressure increases. As shown in Fig. 8d, the volume expansion ratio and half-life time of CO_2 foam layer formed after decompression increases with the increase of equilibrium time. As is known to all, equilibrium pressure and equilibrium time directly affect the amount of CO_2 dissolved in the solution, thus affecting the volume expansion ratio and half-life time of CO_2 foam.

3.5. The interaction between bubbles and ceramsite particles

Achieving perfect particle carry capability is one of the key issues need to be considered for the design of fracture fluid. The interaction between the bubbles and the ceramsite particles was investigated in this section.

Collision adhesion and precipitation adhesion which occur simultaneously are the two ways that bubbles adhere to the surface of the ceramsite particles. The whole process can be divided into four stages: (1) the collision stage between ceramsite particles and bubbles or the precipitation stage of bubbles on the surface of ceramsite particles; (2) the adhesion stage of ceramsite particles and bubbles; (3) the floating stage of gas-solid combination; (4) forming the stable foam layer stage.

In the collision adhesion mode, the interaction between bubbles and ceramsite particles is divided into three stages: (1) the ceramsite particles and the bubbles are close to each other and collide; (2) the hydration film between ceramsite particles and bubbles thins and breaks; (3) ceramsite particles adhere to the bubble surface, that is, the formation and adjustment of interface between ceramsite particles and bubbles. The three-phase contact line will move until the wetted periphery is formed in the collision process. The formation of the wetted periphery increases the contact angle to 135.72°, as shown in Fig. 9a, and produced enough adhesion to prevent ceramsite particles from falling off as shown in Fig. 9b and c.

Precipitation adhesion refers to that during the depressurization process, the microbubbles nucleus precipitate and grow on the surface of the ceramsite particles, forming ceramsite particles-microbubbles complex, as shown in Fig. 9d. Air flocculation groups composed by a plurality of microbubbles and several ceramsite particles can float by the buoyancy of microbubbles as shown in Fig. 9e. The adhesion force of this mode is stronger than the collision adhesion mode between ceramsite particles and bubbles, because the adhesion contact area is larger and the adhesion between ceramsite particles and microbubbles is a gas-liquid direct contact without residual hydration layers.

By adhering to bubbles, ceramsite particles oscillate at the bottom of bubbles, and are desorbed from the bubbles surface by gravity, inertial centrifugal force and fluid force. During the floating process of ceramsite particles-bubbles complex and in the foam layer, the coalescence and rupture of bubbles due to collision with each other also causes desorption.

3.6. Ceramsite suspension capacity of CO_2foam system

Fig. 10a shows the results of the ceramsite static sedimentation test of CO_2 foam at different HMPE solution concentrations within 600 min. It is observed that the suspension capacity of CO_2 foam generated by 0.05 wt% HMPE solution could reach over 65 % at 600 min. As shown in Fig. 10b, the settling velocity of the ceramsite decreases with the increase of HMPE solution concentration due to the viscoelasticity of foam increases. The ceramsite static sedimentation test for CO_2 foam with different load capacity is shown in Fig. 10c. It can be seen that the settling velocity of ceramsite increase with the increase of load capacity. In Fig. 10d, the ceramsite settling velocity as a function of loading capacity is presented. Taking the static sedimentation test results with load capacity of 35% at CO_2 foam generated by 0.10 wt% HMPE solution as an example, the settling velocity calculated is 1.6×10^{-6} m/s. In the fracturing fluid system, the settling velocity of proppant will directly affect the fracture geometry size and fracture conductivity. Ceramsite settling velocity for the CO_2 foam is two orders of magnitude

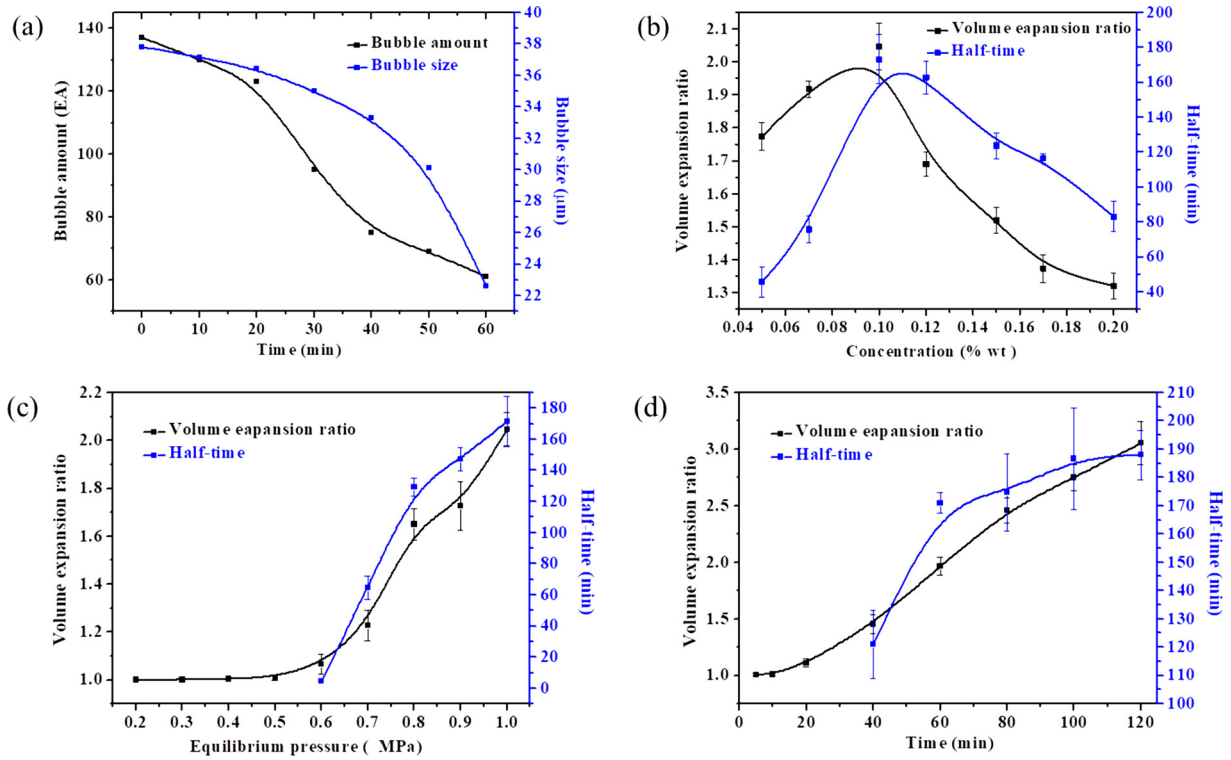

Fig. 8. (a) The bubble amount and bubble size as a function of time; the volume expansion ratio and half-life time of CO_2 foam layer (b) stabilized by HMPE solution as a function of the HMPE concentration at equilibrium pressure of 1 MPa and equilibrium time of 60 min; (c) stabilized by HMPE solution as a function of equilibrium pressure at HMPE concentration of 0.10 wt% and equilibrium time of 60 minutes; (d) stabilized by HMPE solution as a function of equilibrium time at HMPE concentration of 0.10 wt% and equilibrium pressure of 1 MPa.

lower than the maximum permissible proppant settling velocity (8.3×10^{-4} m/s) for fracturing fluids for efficient proppant transportation and placement [46–48].

Images of morphological changes of CO_2 foam carrying ceramsite particles are shown in Fig. 11a. It can be seen that the ceramsite particles will drive the surrounding foam to move downward during the sedimentation process. With the drainage of CO_2 foam, some ceramsite particles aggregate to behave like a large particle, which is equivalent to greatly increasing the diameter of the particle, and the supporting effect of CO_2 foam layer on ceramsite particles gradually weakens, so the settling velocity increases.

Microscopically, the forces exerted on a ceramsite particle included the particle's gravity, the pulling force of films, the resultant pressure force from the adjacent bubbles [49], the viscous force and the frictional force, can prevent the longitudinal movement of ceramsite particles as shown in Fig. 11b. And the CO_2 foam can be moved to a specific position together with the ceramsite because of its structural characteristics. Only when the foam below ceramsite particles are forced through a channel or when the CO_2 foam is badly deformed and extremely unstable, the sedimentation of ceramsite particles will be caused.

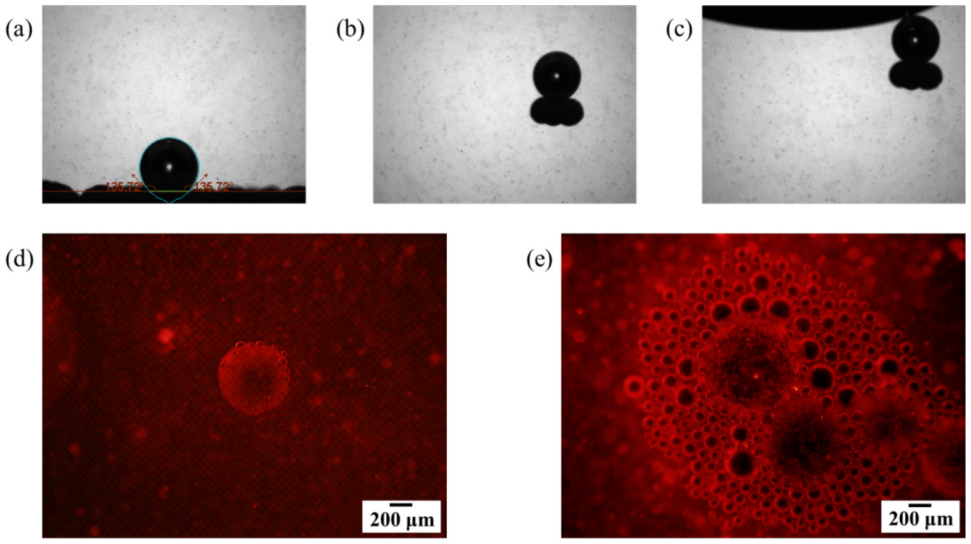

Fig. 9. (a) The contact angle of CO_2 bubble on the surface of the ceramsite particles in the 0.10 wt% HMPE solution; (b) the images of CO_2 bubbles adhering to ceramsite particle surfaces in the 0.10 wt% HMPE solution; (c) the images of CO_2 bubbles adhering to ceramsite particle surfaces at the gas-liquid interface; the fluorescence microscopy images of (d) CO_2 bubbles precipitated adhere to the ceramsite particle surface; (e) air flocculation groups consisting of microbubbles and ceramsite particles.

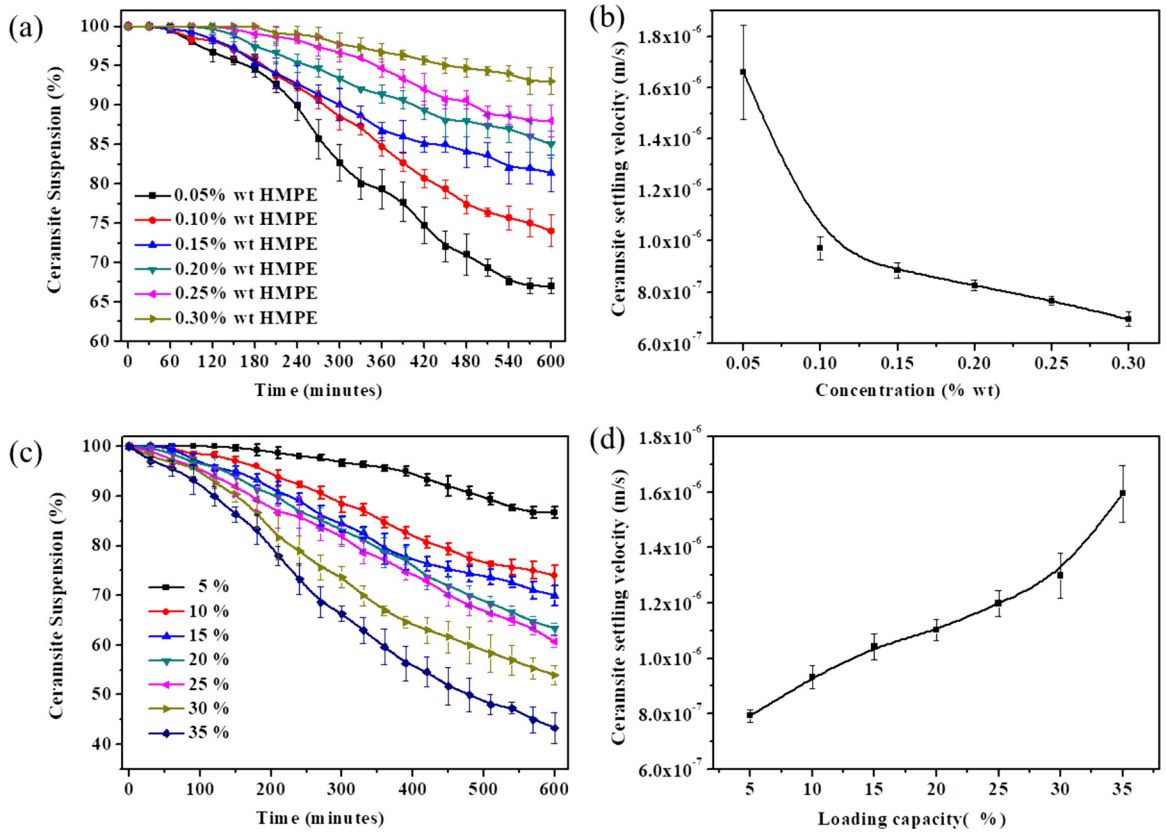

Fig. 10. (a) Ceramsite suspension capacity as a function of time with a fixed loading capacity of 10% at different HMPE solution concentrations; (b) ceramsite settling velocity as a function of concentration with a fixed load capacity of 10%; (c) ceramsite suspension capacity as a function of time with CO_2 foam generated from 0.10 wt% HMPE solution at different load capacity; (d) ceramsite settling velocity as a function of loading capacity with CO_2 foam generated from 0.10 wt% HMPE solution.

4. Conclusion

In this paper, the formation and stabilization of CO_2 bubbles with different sizes stabilized by hydrophobically modified water-soluble polyelectrolyte, i.e. HMPE, was comprehensively investigated. The CO_2 foam produced by HMPE solution exhibited excellent stability, which was related to its strong liquid-holding capacity and prominent elasticity enhanced by the formation of the thick “armor” formed by HMPE

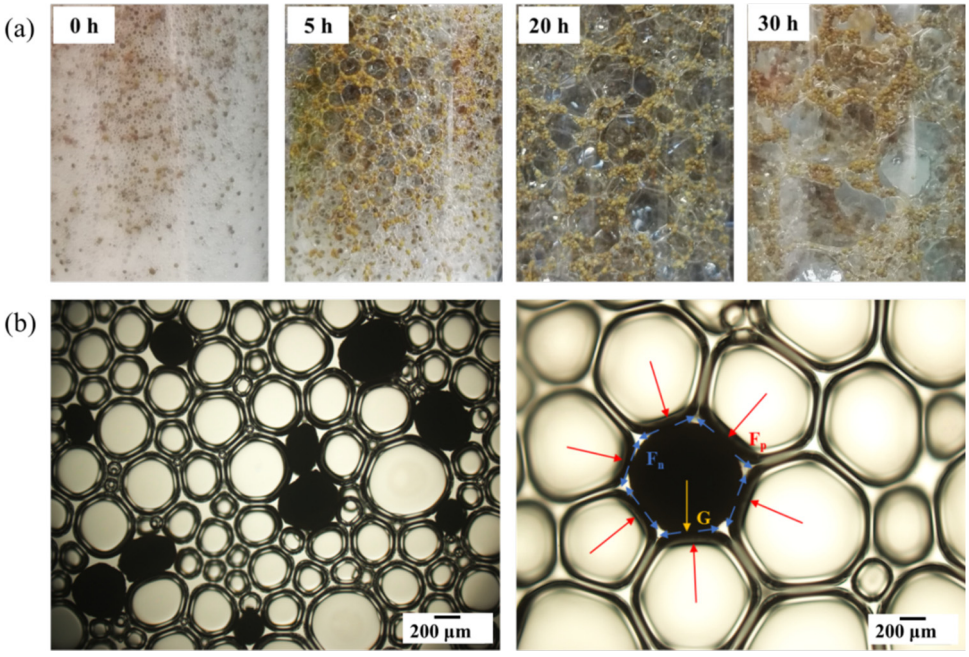

Fig. 11. (a) Images of morphological changes of CO_2 foam carrying ceramsite particles; (b) the interactions between ceramsite particles and CO_2 bubbles.

molecules adsorbed at the gas-liquid interface. Micron-sized CO_2 bubbles were generated by the pressurization-decompression method to surmount the fatal defect of the high frictional resistance for the common foam fluid containing millimeter-sized bubble in the unconventional oil and gas reservoirs with small pore size. The factors affecting the resulted amount of micron-sized CO_2 bubbles were investigated. The mechanism driving CO_2 bubbles adhered to the surface of the ceramsite was discussed, which resulted in the carry capability of the foam films for the ceramsite particles. The HMPE-CO_2 foam exhibited satisfactory ceramsite suspension capacity caused by the forces exerted on a ceramsite particle, of which the settling velocity is two orders of magnitude lower than the common permissible proppant settling velocity for traditional fracturing fluids. Above all, HMPE-CO_2 foam exhibits remarkable performances in all aspects, and could be an ideal candidate for foam flooding or foam fracturing in EOR and EGR.

CRediT authorship contribution statement

Xiaohan Zhang: Data curation, Investigation, Methodology, Validation, Writing - original draft. **Ying Li:** Writing - review & editing.

Declaration of Competing Interest

The authors declare that they have no known competing financial interests or personal relationships that could have appeared to influence the work reported in this paper.

Acknowledgments

This work was financially supported by the National Science Fund of China (No. 21872084, 61575109, 21473103) and the Key Research and Development Project of Shandong Province (No. 2018GSF117025).

References

[1] F. Du, B. Nojabaei, A review of gas injection in shale reservoirs: enhanced oil/gas recovery approaches and greenhouse gas control, Energies 12 (2019) 2355.
[2] P. Nguyen, H. Fadaei, D. Sinton, Pore-scale assessment of nanoparticle-stabilized CO_2 foam for enhanced oil recovery, Energy Fuels 28 (2014) 6221–6227.
[3] C. Zheng, Y. Cheng, Q. Wei, X. Li, Z. Zhang, Suspension of surface-modified nano-SiO_2 in partially hydrolyzed aqueous solution of polyacrylamide for enhanced oil recovery, Colloids Surf. A 524 (2017) 169–177.
[4] S. Rezaei Gomari, Y. Gorra Diallo Omar, F. Amrouche, M. Islam, D. Xu, New insights into application of nanoparticles for water-based enhanced oil recovery in carbonate reservoirs, Colloids Surf. A 568 (2019) 164–172.
[5] D. Kong, Y. Li, M. Yu, R. Ma, H. Guo, Y. Peng, S. Xu, H. Yan, Experimental investigation on block and transport characteristics of foam in porous media for enhanced oil recovery processes, Colloids Surf. A 570 (2019) 22–31.
[6] S. Ahmed, K.A. Elraies, J. Forooozesh, S.R. Bt Mohd Shafian, M.R. Hashmet, I.C.C. Hsia, A. Almansour, Experimental investigation of immiscible supercritical carbon dioxide foam rheology for improved oil recovery, J. Earth Sci. 28 (2017) 835–841.
[7] A.E. Bayat, K. Rajaei, R. Junin, Assessing the effects of nanoparticle type and concentration on the stability of CO_2 foams and the performance in enhanced oil recovery, Colloids Surf. A 511 (2016) 222–231.
[8] S. Kumar, A. Mandal, Investigation on stabilization of CO_2 foam by ionic and nonionic surfactants in presence of different additives for application in enhanced oil recovery, Appl. Surf. Sci. 420 (2017) 9–20.
[9] X. Yin, W. Kang, S. Song, Z. Huang, X. Hou, H. Yang, Stabilization mechanism of CO_2 foam reinforced by regenerated cellulose, Colloids Surf. A 555 (2018) 754–764.
[10] S. Ahmed, K. Elraies, M. Hashmet, A. Hanamertani, Viscosity models for polymer free CO_2 foam fracturing fluid with the effect of surfactant concentration, salinity and shear rate, Energies 10 (2017) 1970.
[11] R. Middleton, H. Viswanathan, R. Currier, R. Gupta, CO_2 as a fracturing fluid: potential for commercial-scale shale gas production and CO_2 sequestration, Energy Procedia 63 (2014) 7780–7784.
[12] Q. Sun, Z. Li, J. Wang, S. Li, B. Li, L. Jiang, H. Wang, Q. Lü, C. Zhang, W. Liu, Aqueous foam stabilized by partially hydrophobic nanoparticles in the presence of surfactant, Colloids Surf. A 471 (2015) 54–64.
[13] C. Zhang, Z. Li, Q. Sun, P. Wang, S. Wang, W. Liu, CO_2 foam properties and the stabilizing mechanism of sodium bis(2-ethylhexyl)sulfosuccinate and hydrophobic nanoparticle mixtures, Soft Matter 12 (2016) 946–956.
[14] W. Pu, P. Wei, L. Sun, S. Wang, Stability, CO_2 sensitivity, oil tolerance and displacement efficiency of polymer enhanced foam, RSC Adv. 7 (2017) 6251–6258.
[15] Y. Zeng, R. Farajzadeh, S.L. Biswal, G.J. Hirasaki, A 2-D simulation study on CO_2 soluble surfactant for foam enhanced oil recovery, J. Ind. Eng. Chem. 72 (2019) 133–143.
[16] C. Li, Y. Huang, X. Sun, R. Gao, F. Zeng, P. Tontiwachwuthikul, Z. Liang, Rheological properties study of foam fracturing fluid using CO_2 and surfactant, Chem. Eng. Sci. 170 (2017) 720–730.
[17] Q. Lv, Z. Li, B. Li, S. Li, Q. Sun, Study of nanoparticle–surfactant-stabilized foam as a fracturing fluid, Ind. Eng. Chem. Res. 54 (2015) 9468–9477.
[18] Q. Lv, Z. Li, B. Li, D. Shi, C. Zhang, B. Li, Silica nanoparticles as a high-performance filtrate reducer for foam fluid in porous media, J. Ind. Eng. Chem. 45 (2017) 171–181.
[19] S. Sun, Y. Wang, C. Yuan, H. Wang, W. Wang, J. Luo, C. Li, S. Hu, Tunable stability of oil-containing foam systems with different concentrations of SDS and hydrophobic silica nanoparticles, J. Ind. Eng. Chem. 82 (2020) 333–340.
[20] W.A.M. Wanniarachchi, P.G. Ranjith, M.S.A. Perera, Shale gas fracturing using foam-based fracturing fluid: a review, Environ. Earth Sci. 76 (2017).
[21] Z. Xue, A.J. Worthen, C. Da, A. Qajar, I.R. Ketchum, S. Alzobaidi, C. Huh, M. Prodanovic, K.P. Johnston, Ultradry carbon dioxide-in-water foams with viscoelastic aqueous phases, Langmuir 32 (2016) 28–37.
[22] Y. Sun, X. Qi, H. Sun, H. Zhao, Y. Li, Understanding about how different foaming gases effect the interfacial array behaviors of surfactants and the foam properties, Langmuir 32 (2016) 7503–7511.
[23] Y. Fei, J. Zhu, B. Xu, X. Li, M. Gonzalez, M. Haghighi, Experimental investigation of nanotechnology on worm-like micelles for high-temperature foam stimulation, J. Ind. Eng. Chem. 50 (2017) 190–198.
[24] H. Farhadi, S. Riahi, S. Ayatollahi, H. Ahmadi, Experimental study of nanoparticle-surfactant-stabilized CO_2 foam: stability and mobility control, Chem. Eng. Res. Des. 111 (2016) 449–460.
[25] F. Guo, S. Aryana, An experimental investigation of nanoparticle-stabilized CO_2 foam used in enhanced oil recovery, Fuel 186 (2016) 430–442.
[26] S. Li, K. Yang, Z. Li, K. Zhang, N. Jia, Properties of CO_2 foam stabilized by hydrophilic nanoparticles and nonionic surfactants, Energy Fuels 33 (2019) 5043–5054.
[27] Z. Xue, A. Worthen, A. Qajar, I. Robert, S.L. Bryant, C. Huh, M. Prodanovic, K.P. Johnston, Viscosity and stability of ultra-high internal phase CO_2-in-water foams stabilized with surfactants and nanoparticles with or without polyelectrolytes, J. Colloid Interface Sci. 461 (2016) 383–395.
[28] B.P. Binks, S. Campbell, S. Mashinchi, M.P. Piatko, Dispersion behavior and aqueous foams in mixtures of a vesicle-forming surfactant and edible nanoparticles, Langmuir 31 (2015) 2967–2978.
[29] A.A. Eftekhari, R. Krastev, R. Farajzadeh, Foam stabilized by fly ash nanoparticles for enhancing oil recovery, Ind. Eng. Chem. Res. 54 (2015) 12482–12491.
[30] D. Lee, H. Cho, J. Lee, C. Huh, K. Mohanty, Fly ash nanoparticles as a CO_2 foam stabilizer, Powder Technol. 283 (2015) 77–84.
[31] Q. Lv, Z. Li, B. Li, M. Husein, S. Li, D. Shi, W. Liu, H. Bai, L. Sheng, Synergistic mechanism of particulate matter (PM) from coal combustion and saponin from Camellia seed pomace in stabilizing CO_2 foam, Energy Fuels 32 (2018) 3733–3742.
[32] O. Rahmani, Mobility control in carbon dioxide-enhanced oil recovery process using nanoparticle-stabilized foam for carbonate reservoirs, Colloids Surf. A 550 (2018) 245–255.
[33] A.S. Emrani, H.A. Nasr-El-Din, An experimental study of nanoparticle-polymer-stabilized CO_2 foam, Colloids Surf. A 524 (2017) 17–27.
[34] H. Li, J. Zhao, A. Wang, Q. Li, W. Cui, Supramolecular assembly of protein-based nanoparticles based on tumor necrosis factor-related apoptosis-inducing ligand (TRAIL) for cancer therapy, Colloids Surf. A 590 (2020).
[35] H. Li, Y. Zhao, Y. Jia, C. Qu, J. Li, Covalently assembled dopamine nanoparticle as an intrinsic photosensitizer and pH-responsive nanocarrier for potential application in anticancer therapy, Chem. Commun. (Camb.) 55 (2019) 15057–15060.
[36] X. Xu, A. Saeedi, K. Liu, Laboratory studies on CO_2 foam flooding enhanced by a novel amphiphilic ter-polymer, J. Petrol. Sci. Eng. 138 (2016) 153–159.
[37] G. Zhao, C. Dai, Y. Zhang, A. Chen, Z. Yan, M. Zhao, Enhanced foam stability by adding comb polymer gel for in-depth profile control in high temperature reservoirs, Colloids Surf. A 482 (2015) 115–124.
[38] Q. Lv, T. Zhou, X. Zhang, R. Zheng, C. Zhang, B. Li, Z. Li, Dynamic filtration behavior of dry supercritical CO_2 foam with nanoparticles in porous media, Ind. Eng. Chem. Res. 58 (2019) 15014–15025.
[39] S. Alzobaidi, M. Lotfollahi, I. Kim, K.P. Johnston, D.A. DiCarlo, Carbon dioxide-in-brine foams at high temperatures and extreme salinities stabilized with silica nanoparticles, Energy Fuels 31 (2017) 10680–10690.
[40] A.S. Emrani, H.A. Nasr-El-Din, An experimental study of nanoparticle-polymer-stabilized CO_2 foam, Colloids Surf. A 524 (2017) 17–27.
[41] A. Verma, G. Chauhan, K. Ojha, E. Padmanabhan, Characterization of nano-Fe_2O_3-stabilized polymer-free foam fracturing fluids for unconventional gas reservoirs, Energy Fuels 33 (2019) 10570–10582.
[42] 李英, 吕韦钦, 李德春, 一种水基泡沫稳定剂、制备方法及具有超高稳定性的水基泡沫体系.
[43] S. Li, Z. Li, P. Wang, Experimental study of the stabilization of CO_2 foam by sodium dodecyl sulfate and hydrophobic nanoparticles, Ind. Eng. Chem. Res. 55 (2016) 1243–1253.
[44] S. Li, C. Qiao, Z. Li, S. Wanambwa, Properties of carbon dioxide foam stabilized by hydrophilic nanoparticles and hexadecyltrimethylammonium bromide, Energy Fuels 31 (2017) 1478–1488.
[45] X. Hu, Y. Li, X. He, C. Li, Z. Li, X. Cao, X. Xin, P. Somasundaran, Structure–behavior–property relationship study of surfactants as foam stabilizers explored by experimental and molecular simulation approaches, J. Phys. Chem. B 116 (2011) 160–167.
[46] A. Verma, G. Chauhan, P.P. Baruah, K. Ojha, Morphology, rheology, and kinetics of nanosilica stabilized gelled foam fluid for hydraulic fracturing application, Ind. Eng.

Chem. Res. 57 (2018) 13449–13462.
[47] X. Luo, S. Wang, Z. Wang, Z. Jing, M. Lv, Z. Zhai, T. Han, Experimental investigation on rheological properties and friction performance of thickened CO_2 fracturing fluid, J. Petrol. Sci. Eng. 133 (2015) 410–420.
[48] A. Verma, G. Chauhan, K. Ojha, Synergistic effects of polymer and bentonite clay on rheology and thermal stability of foam fluid developed for hydraulic fracturing, Asia-Pac. J. Chem. Eng. 12 (2017) 872–883.
[49] Y. Fei, K. Pokalai, R. Johnson, M. Gonzalez, M. Haghighi, Experimental and simulation study of foam stability and the effects on hydraulic fracture proppant placement, J. Nat. Gas Sci. Eng. 46 (2017) 544–554.